Computers in Biology and Medicine 189 (2025) 109912

Contents lists available at ScienceDirect

Computers in Biology and Medicine

journal homepage: www.elsevier.com/locate/compbiomed

Facial characteristics description and classification based on 3D images of Fragile X syndrome in a retrospective cohort of young Chinese males

Jieyi Chen [a,b,1], Siyuan Du [b,1], Yiting Zhu [c,1], Dongyun Li [c], Chunchun Hu [c], Lianni Mei [c], Yunqian Zhu [a], Huihui Chen [a], Sijia Wang [d], Xiu Xu [c], Xinran Dong [a,*], Wenhao Zhou [a,e], Qiong Xu [c]

[a] Center for Molecular Medicine, Pediatrics Research Institute, Children's Hospital of Fudan University, Shanghai, China
[b] Bio-X Institutes, Key Laboratory for the Genetics of Developmental and Neuropsychiatric Disorders, Ministry of Education, Shanghai Jiao Tong University, Shanghai, China
[c] Child Health Care Department, Children's Hospital of Fudan University, Shanghai, China
[d] CAS Key Laboratory of Computational Biology, Shanghai Institute of Nutrition and Health, University of Chinese Academy of Sciences, Chinese Academy of Sciences, 320 Yue Yang Road, Shanghai, China
[e] Guangzhou Women and Children's Medical Center, Guangzhou Medical University, Guangzhou, China

A B S T R A C T

Purpose: Fragile X syndrome (FXS) is a common cause of intellectual disability and autism. FXS presents with abnormal facial features, which in pediatric patients are subtler than what is seen in adults. The three-dimensional (3D) facial images, which contain more stereoscopic and subtle information than two-dimensional (2D) photographs, are increasingly being used to classify genetic syndromes. Here, we used 3D facial images to describe facial features and construct a classification model, especially in male patients with FXS.

Methods: We registered the 3D facial images of 40 Chinese boys with FXS and 40 healthy boys. We utilized seven machine learning models with different features extracted from dense point cloud and sparse landmarks. A linear regression model was performed between feature reduction of regional point cloud and genomic as well as methylation subtypes.

Results: The typical and subtle differences between 3D average faces of patients and controls could be quantitatively visualized. The projection of patients and controls in Fragile X-liked vectors are significantly different. The random forests model using coordinates of regional facial points (chin, eye, forehead, nose and upper lip) could perform better than expert clinicians in binary classification. Among the 63 hierarchical facial segmentation, significantly associations were found in 8 segments with genetic subtypes, and 2 segments with methylation subtypes.

Conclusion: The 3D facial images could assist to distinguish male patients with FXS by machine learning, in which the selected regional features performed better than the global features and sparse landmarks. The genetic and methylation status might affect regional facial features differently.

1. Introduction

Fragile X syndrome (FXS) is the most prevalent inherited cause of intellectual disability [1]. While FXS can affect both genders, males are more commonly and severely affected compared to females [2]. It is associated with symptoms such as intellectual disability, behavioral and learning challenges, features of autism spectrum disorders, and various physical characteristics [3]. Facial features unique to FXS include a long and narrow face (HP:0000275, HP:0000276), broad forehead (HP:0002003), mandibular prognathism (HP:0000303) and protruding ear (HP:0000411) [4]. Some other occasional facial morphological features, like thin and long palpebral fissures, puffiness around the eyes, epicanthal folds and broad nose, were observed and described by only a few studies with small sample size [5–7]. Among these and other researches on facial phenotypes, the way for identification and quantification has evolved from manual observation and direct measurements to extracting quantitative and detailed geometric features by digital images, including two-dimensional (2D) and three-dimensional (3D) images. As most individuals involved in studies of FXS are post pubertal or in adulthood and without digital images, the recognizable or subtle facial features at a young age were not well studied. Absence of digital studies in pediatric patients limited the ability to identify early Fragile X facial features.

In recent years, numerous studies have utilized 2D facial images with

* Corresponding author.
E-mail addresses: xrdong@fudan.edu.cn (X. Dong), zhouwenhao@fudan.edu.cn (W. Zhou), xuqiong@fudan.edu.cn (Q. Xu).
[1] Jieyi Chen, Siyuan Du and Yiting Zhu contributed equally to this work.

https://doi.org/10.1016/j.compbiomed.2025.109912
Received 24 May 2024; Received in revised form 18 February 2025; Accepted 20 February 2025
Available online 2 March 2025

deep learning methods or 3D ones with machine learning models to classify distinct genetic syndromes with special facial phenotypes [8,9]. In specific syndromes, machine-assisted screening models performed well, even better than human experts, showing the potential to aid disease diagnosis. Additionally, 3D facial images could be more advantageous than 2D by providing more stereoscopic information [10]. However, due to factors such as limited sample sizes, variations in age distribution, population diversity, and differences in the classification objectives of the models, the accuracies of classification models for FXS were limited [8,9,11]. Therefore, using 3D images might potentially optimize the screening models for Fragile X patients within specific populations and ages.

The primary cause of FXS is a trinucleotide CGG expansion in the promoter region of the Fragile X Messenger Ribonucleoprotein 1 (*FMR1*) gene. The *FMR1* gene is categorized into four types based on the length of CGG repeats: individuals with 6–44 CGG repeats are considered normal, 45–54 CGG repeats are termed "grey zone," premutation (PM) alleles fall within the range of 55–200 CGG repeats, and CGG repeats >200 are designated as full mutations (FM) and are typically methylated [12]. Size mosaicism of the CGG repeats has been observed in many patients with FXS. Males with mosaic mutation of PM and FM have generally been reported to exhibit better intellectual functioning compared to those with FM alone [13]. Besides genomic mutations, the methylation mosaicism was reported to be associated with better cognitive functioning and adaptive behavior and less social impairment [14]. In addition, several physical phenotypes, including decreasing body height, limb length, increased face height and ear width, were also related to deficit of the Fragile X mental retardation protein (FMRP) [15]. Thus, the stereoscopic and quantitative facial phenotypes extracted from 3D images could provide possibility to explore the existence of relationship between subtle facial phenotypes and genotypes, including genomic mutations and methylation.

In this study, we have depicted more subtle facial features of patients through the comparison and quantitative analysis of 3D images from FXS patients and controls at early childhood. Additionally, we explored how to better assist screening by machine learning utilizing 3D facial images. Furthermore, we have investigated whether different genetic genotypes and methylation subtypes in patients affect facial morphology.

2. Materials and methods

2.1. Sample ascertainment and study design

From January to December 2023, we recruited a group of 40 Chinese boys genetically diagnosed as FXS. For the case-control study, we then recruited 40 healthy boys with a similar age distribution to the FXS boys, who were without intellectual or physical developmental delay. All participants received a clinical assessment and explanation of informed consent by specialists from department of child health care. The study protocol approved by the Children's Hospital of Fudan University (FDCH_2022_260 and FDCH_2023_175).

2.2. 3D facial image collection and preprocess

We used VECTRA H1 system (Canfield, Parsippany, NJ) for 3D facial imaging from all participants, including 40 patients and 40 controls. The VECTRA H1 system consists of a VECTRA H1 3D camera with stereo optics and a software running in Windows. The participants were asked to close their mouth, open their eyes and hold faces with a neutral expression. We captured three images from right side, front and left side the VECTRA H1 3D camera, and ensured consistent participant positioning. Then the three images were stitched as a 3D image in the VECTRA software. Each patient was sampled three times. The 3D surface images were registered to a anthropometric mask consisted of 7906 spatially dense points, and were standardized using generalized Procrustes analysis (GPA) and symmetrization to eliminate the influences of position, orientation, and the centroid size of the images [16,17]. Finally, average face of the three measurements for each sample was used for subsequent analysis.

2.3. FXS liked vector and projection

First, we calculated the average face for both the controls ($\overline{F_{Control}}$) and FXS patients ($\overline{F_{FXS}}$). Subsequently, by subtracting the coordinates of the control average face from the coordinates of the FXS average face, we obtained the FXS liked vector (*FXS_v*).

$$FXS\_v = \overline{F_{FXS}} - \overline{F_{Control}}$$

Finally, we projected face coordinate (F_i) of each sample onto this vector, with the length of the vector projection (l_i) indicating the degree to which it resembled the facial morphology of FXS.

$$l_i = \frac{F_i \times FXS\_v}{|FXS\_v|}$$

2.4. Facial landmarking & anatomical regions segmentation

Since previous studies on syndrome classification used sparse landmarks as 3D facial phenotypes, we auto-landmarked 13 facial anatomical landmarks in this study using the dense corresponding approach proposed by White et al. [16] (Supplementary Fig. S1a). By referring to the partitioning methods in previous studies [17,18] and the visualized differences between average faces of the FXS boys and the controls, we divided the global face into nine anatomical regions for further analysis on features of regional face (Supplementary Fig. S1b).

2.5. Classification models by machine learning

To distinguish faces of FXS boys and controls, we used machine learning methods to make binary classification models. We tested seven machine learning approaches, including k-nearest neighbors (KNN), support vector machine (SVM) with linear function or radial basis function (rbf), random forests, and Boosting tree algorithms (including AdaBoost, GBDT and XGB class) by scikit-learn in Python. Due to the limited sample size, we used leave-one-out cross-validation (LOOCV) for internal validation. Our analysis reports accuracy, sensitivity, specificity and F1-score to show performance of each model.

We defined the input features of classification models in four ways. "All_points" is consisted with 23,718-length arrays of the coordinates of 7906 spatially dense points. "Landmark" is consisted with 39-length arrays of the coordinates of 13 sparse anatomical points. "Distances_LM" is consisted with sets of 78 paired linear distances was calculated from those 13 landmarks. The fourth one is consisted with ergodic combination of nine anatomical regions, 510 groups in all, except the global face (Supplementary Table S3). Besides facial information above, the age of every sample was also used as input feature in each model.

To evaluate the performance of the machine learning models, we recruited three expert clinicians from the child health care department to established an "Expert classifier". Each clinician independently reviewed the original 3D texture images of 80 participants and provided a binary classification (FXS or control) for each image (Supplementary Table S1). In the averaged results ('Clinician_avg'), if two or more clinicians classified a sample as FXS, it was considered a positive case. Otherwise, it was classified as a control.

2.6. Phenotyping of dense landmarks

We first corrected the symmetrized facial shapes for the covariates of age and age squared using a partial least-squares regression (PLSR, function plsregress from MATLAB 2018a). In each segment, we

performed principal component analysis (PCA) on the PLSR residuals of the discovery cohort and obtained principal component (PC) scores as the phenotypic scores. The 63 hierarchical facial segmentations derived in Zhang et al. could represent facial phenotypes in global and regional levels. The PC scores of 63 facial segmentations were used for association analysis.

2.7. Genetic and methylation testing

We were allowed to collected peripheral blood samples from 37 patients for genetic and methylation testing.

The *FMR1* CGG repeats testing utilized the PCR-CE *FMR1* Kit (Biofast Biotechnology Co., Ltd.), and capillary electrophoresis (CE) conducted on the ABI 3500 Dx Genetic Analyzer (Thermo Fisher Scientific, Waltham, MA) using 1200 LIZ™ Size Standard, following the manufacturer's instructions. Gene-specific primers annealing to the upstream region in *FMR1* 5′UTR determined CGG repeats, and the triplet-repeated primer targeting the CGG region revealed AGG interruption status. The larger amplicon in *FMR1* 5′UTR covered the full expansion lengths and was converted into CGG repeat numbers using a regression curve derived from a standard mixture, and the CGG stutter amplicon indicated the status of AGG interruptions.

Methylation status was assessed using the PCR-CE m*FMR1* assay (Biofast) according to manufacturer guidelines. gDNA, methylation-sensitive plasmid, and a reference control were pooled, then separated into control and methylation-digested groups. The latter was treated with *Hpa*II then amplified with FAM-labeled primer, while the control group's allele was amplified with NED-labeled primers. Both amplicons were pooled for capillary electrophoresis. The methylation percentage for each allele was calculated by normalizing against the reference control using the equation:

$$\text{Methylation}\ (\%) = 100 \times \frac{\text{FAM labeled}\ ((\text{FMR1 height})/(\text{RefControl height}))}{\text{NED labeled}\ ((\text{FMR1 height})/(\text{RefControl height}))}$$

2.8. Association analysis between phenotype and subtypes

According to CGG repeat numbers tested, all patients in this study could be classified into two subtypes of "PM-FM mosaic" (carrying both 55–200 CGG repeats and CGG repeats >200) and "FM-only" (only carrying CGG repeats >200). "The genetic status" of "PM-FM mosaic" and "FM-only" were respectively equal to "1" and "2".

Referring to methylation percentage all patients in this study could be classified into two subtypes of "partial methylation" (<80 %) and "complete methylation" (≥80 %). "The methylation status" of "partial methylation" and "complete methylation" were respectively equal to "1" and "2".

Since the PC scores are high-dimensional, we utilized the genetic/methylation status as dependent variable and facial PCs as independent variables in linear regression model, with $P < 0.05$ indicating nominal significance. We also used the 10000-times permutation tests to calculate the Bonferroni multiple testing threshold. For permutation in each face segment, we generated the null distribution as follows: 1. Keep the shape PC scores fixed and randomly permute the genotypes/methylation classifications. Note that the PCs between face segment were not completely independent, thus we kept the permutation the same for each segment the same to keep the correlation between facial segments. 2. Perform the association analysis between random genotype/methylation classifications with face PCs in each face segment to calculate p-values. 3. Construct the null p-value distributions in each face segment, and compared the 5 % quantile of the null distribution with 0.05 to identify whether this method will inflate the p-values. 4. Calculate the minimum p-value (minP) among 63 face segments in each permutation. Then, construct the null distribution using the minP in each permutation. Finally, the 5 % quantile of the minP as the Bonferroni threshold. The p-values of multivariate association analysis were not inflated in each face segment for both genetic status (Supplementary Fig. S2a) and methylation (Supplementary Fig. S2c). And besides the nominal p-value threshold of 0.05, we set the Bonferroni threshold as $P = 0.0015$ for genetic status (Supplementary Fig. S2b) and $P = 0.00139$ for methylation (Supplementary Fig. S2a).

3. Results

3.1. Patient characteristics and sample description

With recruitment of 40 FXS boys with confirmed *FMR1* FM, 40 male controls with matched-age were obtained from an existing collection into this study (detailed breakdown of enrollment age in Supplementary Table S1, $P = 0.137$, one-tailed *t*-test). All individuals reported are Chinese of East-Asian origin.

Among all 40 FXS boys, we successfully collected blood samples from 37 patients for gene testing of *FMR1* and methylation analysis (Table 1, detailed information in Supplementary Table S2). According to classification criteria of CGG repeat numbers in *FMR1* gene, there are 17 patients carrying only FM (FM-only), while 20 carrying FM and PM (PM-FM mosaic).

3.2. Comparison of average 3D faces of boys with FXS and healthy controls

The average 3D face of 40 boys with FXS and that of 40 age-matched male controls are respectively shown in Fig. 1 a&b. By calculating the difference in normal vector distances at corresponding points, the degree of facial feature differences, in terms of prominence and concavity, between average faces of patients and controls is respectively using a gradient of red and blue colors in the heatmap (Fig. 1c).

The well-known FXS facial features, such as the long and narrow face, is also dominant in 3D facial visualization. Other reported facial features, including mandibular prognathism, puffiness around the eyes and broad nose, could also be broadly observed in the 3D facial comparison. Besides known facial features mentioned above, a prominent mouth consisted of prominent philtrum and hypotonic droop of the lower lip could be observed. Moreover, the maxillary and nasolabial fold regions showed a tendency to be concave. These observations from 3D facial comparison described more subtle facial features of FXS patients in an extended way.

The differ-vector of average 3D faces could also describe overall difference between patients and controls. We defined the differ-vector of average 3D face from control to FXS as "FragileX-liked vector". By projecting 3D face of each individual to the "FragileX-liked vector", the similarity tendency to patient or control could be assessed quantitatively by the projection value. Unsurprisingly, there are significant differences in the projection values between the patients and the control group (Fig. 2a, $P = 8.40 \times 10^{-10}$, one-tailed *t*-test). In a random permutation test conducted 10,000 times, the difference of mean projection values

Table 1
Sample characteristics.

		Patients	Control
Total	N	40	40
	Age (median, IQR)	5.65 (3.88, 8.71)	5.65 (3.87, 6.54)
	Age range	1.23–14.83	1.69–11.63
***FMR1* mutations**	N	37	–
PM-FM mosaic	N	17	–
	Age (median, IQR)	5.37 (3.86, 7.41)	–
	Age range	2.19–10.54	–
FM-only	N	20	–
	Age (median, IQR)	5.05 (3.80, 8.75)	–
	Age range	1.23–14.83	

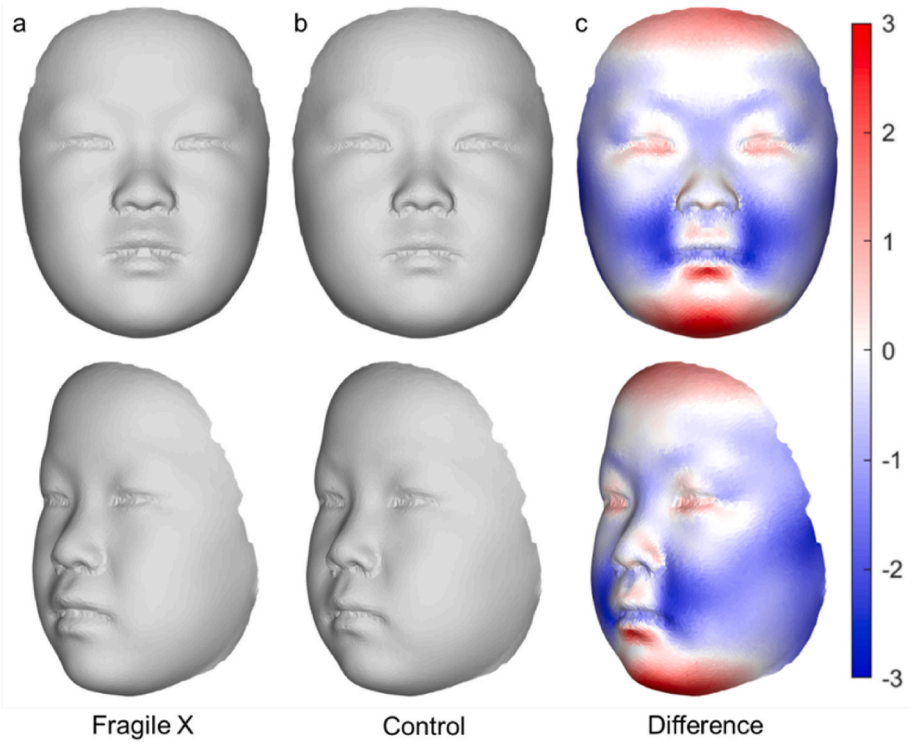

Fig. 1. Average 3D faces of Fragile X patients and healthy controls
3D face visualization images with frontal and lateral 45 degrees of a) Fragile X patients and b)healthy controls. c) Heat maps of position difference with respect to normal axes for densely corresponded points on surface of average of individuals with Fragile X syndrome compared with corresponding position on the average of healthy male controls. The red–white–blue range reflects displacement parallel to the normal axis concerned with maximal red–blue at 3 SD in opposing directions and white at 0 SD. Red represented direction to outside (prominence), and blue represented direction to inside (concavity). (For interpretation of the references to color in this figure legend, the reader is referred to the Web version of this article.)

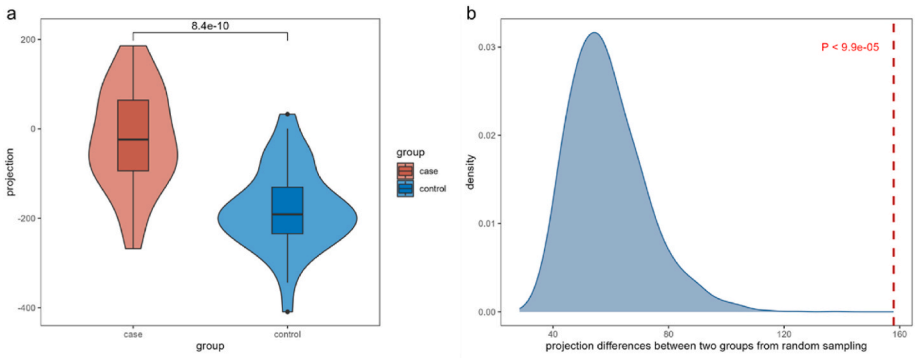

Fig. 2. The distribution of projection on FragileX-liked vector. a) Violin plots and boxplots described the projection distribution of two groups on the FragileX-liked vector. b) The null distribution of differences between two mean projections from 10000 times random sampling and grouping from all samples. The dashed line represented the difference between mean FragileX projection and mean control projection.

between the patients and the control group remained the largest (Fig. 2b, $P < 9.9 \times 10^{-5}$). This indicates that the differences observed between the patients and the controls are indeed significant.

3.3. Using 3D facial images to distinguish patients and controls

The analysis presented above demonstrated visual differences between 3D average faces of FXS boys and controls, as well as significant quantitative differences in the projection analysis. These findings and previous studies on machine-assisted classification suggested the potential for using 3D facial images to construct a specific binary classification model for FXS boys and controls.

In order to investigate phenotypes most suitable for the model use, we explored different kinds of points information from 3D facial data as input features (Supplementary Table S3). The performance of models using input feature of "All_points" is better than those using "Landmark" and "Distances_LM", suggesting dense points with more information is better than sparse landmarks. However, when using 510 groups of different combinations from nine anatomical region as input features, several models performed better than "All_points", indicating that the features of regional face is enough to distinguish patients and controls.

Among all seven machine learning algorithms used in this study, we compared the accuracies, sensitivity, specificity and F1-score of all models between each two algorithms (paired one-tailed *t*-test, Supplementary Table S4). The random forest algorithms performed better every other machine learning algorithm in all four indicators. The SVM

with linear function is second only to random forest algorithm.

Finally, we selected the models with the best performance of each kind of input features, with the best one from 510 groups of different combinations (Table 2). All of the selected machine learning models performed better than the "expert classifier", expect the sensitivity. The random forest model using points of the group C5-95, including the regions of chin, eye, forehead, nose and upper lip, could reach the highest accuracy as 0.9. This indicated that the suitable machine learning model using regional facial points cloud match or even surpass the performance of expert clinicians in distinguish FXS patients from controls.

3.4. Regional facial phenotypes correlated with genetic classification of FXS

The facial phenotypic differences between patients and controls can indeed be regarded as extreme differences between disease and non-disease states. Within FXS boys, it is widely recognized that individuals carrying FM may present more severe symptoms compared to those exhibiting PM/FM mosaicisms. Therefore, we conducted further investigations in 37 patients only, to explore whether the genetic classification based on CGG repeat numbers also influences facial phenotypes in global or regional levels, similar to what observed in patients and controls. Meanwhile, in recent studies, the relationship between the methylation status of *FMR1* and the severity of symptoms has been investigated.

We performed association analysis between PCs of each 63 regions and the genetic/methylation status (Fig. 3, Supplementary Table S4). Three segments ($P_{Seg20} = 0.0486$, $P_{Seg40} = 0.0354$ and $P_{Seg45} = 0.0480$), which also could be included in chin and lower jaw regions, were found to be associated with the genetic status at nominal significant level. Since the facial development showed an inflection point in the previous study, we further analyzed in two age group divided by 5-year-olds [19]. Four segments ($P_{Seg9} = 0.0244$, $P_{Seg17} = 0.0276$, $P_{Seg39} = 0.0161$ and $P_{Seg55} = 0.0122$) and one segment ($P_{Seg35} = 0.00110$) were associated with the genetic status in the <5 years group at nominal and Bonferroni significant level respectively. These facial segments were located in the nose region and partial cheek near nose. However, no association with the genetic status was found in the ≥5 years group.

In analysis with the methylation status, two segments ($P_{Seg47} = 0.0358$ and $P_{Seg50} = 0.0322$) showed association at nominal significant level. The Seg50, representing the eye region was also associated with the methylation status in the ≥5 years group at nominal significant level ($P_{Seg50} = 0.0310$). There was no other significant association with the methylation status was found in all samples or two age groups. These results suggested regional facial phenotypes might be influenced by genetic factor and the methylation of *FMR1* in different ages.

4. Discussion

This study investigated the facial characteristics of FXS patients using 3D facial imaging and explored the potential of using these features to distinguish patients from controls. The findings revealed significant visual and quantitative differences between the average 3D faces of patients and controls. Machine learning models using different input features demonstrated the potential for constructing a binary classification model for FXS patients and controls based on 3D facial images. Facial regions divided based on visual differences, particularly the combination of chin, eye, forehead, nose and upper lip regions, showed promising results in distinguishing patients from controls. Furthermore, the study examined the association between facial phenotypes and genetic classification within FXS patients, revealing significant associations between specific regional facial features and the genetic and methylation status.

This study extensively utilized 3D facial imaging to investigate the phenotypic patterns and applications in FXS patients, yielding constructive conclusions, but also had some limitations. First, the original 3D facial images collected did not include the complete ear region, and the registration mask face also lacked the ear portion. Therefore, the well-known feature of protruding ear is not available in this study to be visualized or analyzed with genotypes. Although the sample size of patients is generally larger than other studies including facial phenotypes of FXS, the cohort with only 40 case-control pairs of young age is still not enough to summarize complete facial features and developmental patterns of patients. Nevertheless, 3D facial images repeated the exhibit facial features of FXS and described more subtle features, indicating the adding value of 3D data to explore phenotypes in young patients.

While the use of 3D facial imaging and machine learning techniques showed promise in distinguishing FXS patients from controls, there are several limitations to consider. Facial features could be influenced by various external factors such as age, facial expression and ethnic background. However, during image capture, we controlled these external factors into a stable status, including the finite age distribution of perfect matches and all East-Asian origin individuals. Machine learning models trained on a specific dataset might have the potential to overfit, without the generalizability to different age and ethnic background. We only used LOOCV as internal validation in a small dataset; larger sample size could validate the performance of models in an independent dataset. On the other hand, we used different combinations of facial landmarks and regions as input features to explore more suitable features for machine learning. We found that the model using regions of chin, eye, forehead, nose and upper lip as input feature performed best in this study, which is consist with the different regions between average faces of controls and patients (Fig. 1c). This is probably because the regions with obviously differences played a more important role, while the regions with no difference might be confounders reducing model performance. In addition to using regional feature in machine learning models of classification between patients and controls, the more ways of feature extracting could be tested in the future, like the 65 landmarks used before [9]. Referring to transform learning often used in 2D image research, the deep hierarchical feature learning method could be used for 3D feature extraction before classification model construction. In all, for child health care departments with a large number of patients or a lack of experienced doctors, machine-assisted disease screening is a practical help to improve operational efficiency and diagnostic accuracy. Although this study only established a binary classification model for males with FXS, it demonstrated the application potential of 3D facial images in auxiliary screening. The future collection of more samples of different sex, age and ethnic could validate whether the

Table 2
Performance of binary classification models using different types of input features with algorithms.

Input_feature	Textrue_image	All_points	Landmark	Distances_LM	C5-95[a]
Machine learning algorithm	Expert classifier	Random Forest	Random Forest	Random Forest	Random Forest
Accuracy	0.812	0.863	0.838	0.812	0.9
Sensitivity	1	0.9	0.9	0.825	0.9
Specificity	0.625	0.825	0.775	0.8	0.9
F1-score	0.769	0.857	0.827	0.81	0.9

[a] C5-95 represented the regions of chin, eye, forehead, nose and upper lip.

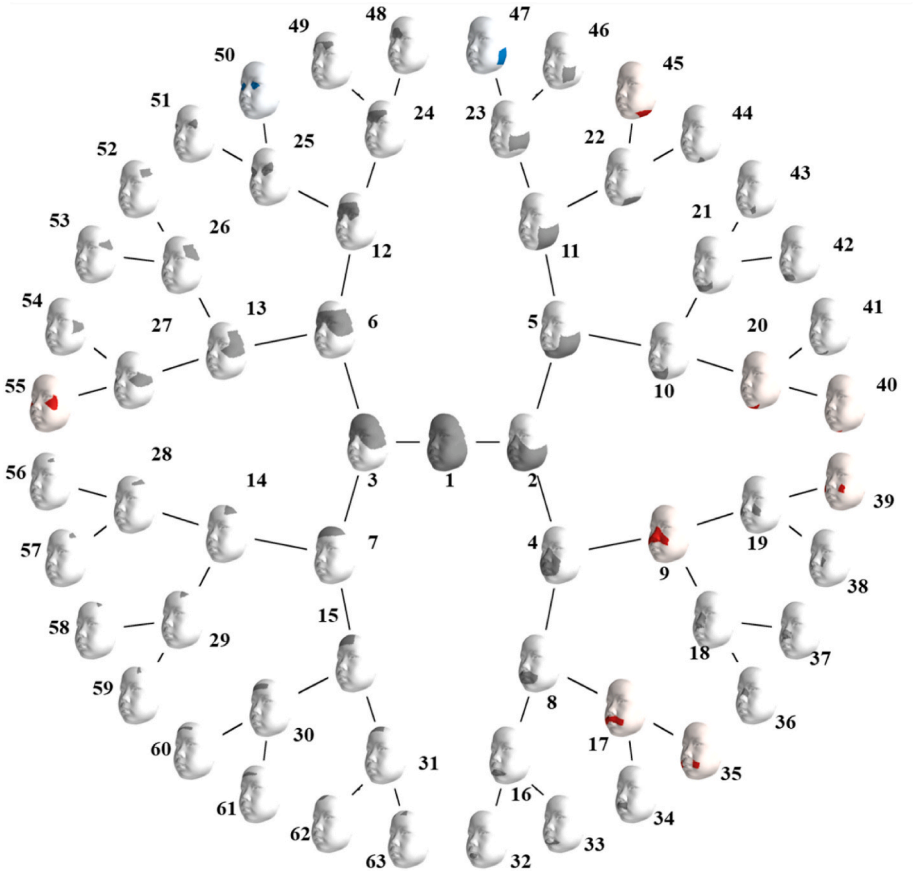

Fig. 3. The hierarchical facial segmentation.
Facial shape variation is covered at five different levels of detail, same as the previous study. Segments are colored in grey. The segments significantly associated with the genetic and methylation status were respectively highlighted by red and blue. (For interpretation of the references to color in this figure legend, the reader is referred to the Web version of this article.)

model in this study is applicable to non-Chinese boys and female patients. In addition, since many patients with neurogenetic syndromes presenting with ID and/or ASD require accurate and rapid diagnosis, we would collect more 3D facial images of patients with other diseases for the construction of multi-classification or other disease specific binary classification models. More feature extraction methods are also planned to increase generalizability of classification models.

Finally, we explored association analysis between regional facial phenotypes and genotypes, including genetic status and methylation status. The finding of significant associations suggested that the genetic mutation and the methylation level of the *FMR1* gene might affect different facial morphological phenotypes. The Seg 20, 40 and 45 showed the FM-only patients were with a more obtuse chin and a little wider lower jaw based on a longer and narrower face (Supplementary Fig. S3). Interestingly, although the phenotypes of midface showed no association with the subtype defined by the number of CGG repeats, those showed significant association among patients <5 years group. The five relevant segments could be summarized as a more concave infraorbital and nasolabial fold region in FM-only patients. The former facial structure might be consisted with a narrow sinus ostium and related to the recurrent sinusitis common in FXS patients [20,21]. Meanwhile, the midface region near nose undergo a more rapid growth rate <5 years group than other regions, so this phenomenon suggests that the number of CGG repeats might affect the speed of facial development in early childhood [18,19,22]. However, in later stages of development, due to the slow growth rate and the same developmental end points, the facial morphology associated with the number of CGG repeats becomes less obvious. Meanwhile, the eye region is more prominent in patients with the higher methylation status, both in the whole age group and ≥5 years group. The power of associations found in this study were limited by sample size and simplified subtypes. The methylation status was also limited by the samples collected from peripheral blood, rather than tissues directly related to facial morphology. Additionally, increased intragenic DNA methylation of the CpG island and the Fragile X Related Epigenetic Element 2 (FREE2) is correlated with lower intellectual functioning in both males and females with FXS, which even could support the prediction of intellectual functioning and autism features in male patients [13,23,24]. Moreover, in females with PM, higher level of DNA methylation at FREE2 was reported to be associated with neuro-phenotypes, which also suggested the association between epi-genotypes and volume of white matter in female carriers and patients [25,26]. In sum, these correlation findings could give insight to pathogenic mechanism and suggestive features in computer aided diagnosis models for subtypes of FXS. In the future, more genetic or epigenetic tests such as long read sequencing to obtain the exact CGG repeats, FMRP level, refined methylation subtyping and tissue specific methylation can also be included to further investigate the association between facial phenotypes and genotypes, not only in male patients but also in female patients and PM carriers.

In conclusion, this study demonstrates the potential of using 3D images to reveal specific and subtle facial characteristics of FXS in young age groups. The findings contribute to our understanding of the relationship between genotypes and phenotypes in FXS and highlight the importance of considering regional facial features in diagnostic models. Future studies should aim to validate these findings in larger and more diverse cohorts and investigate additional genetic or epigenetic factors that may influence facial phenotypes.

Research ethical statement

This study was conducted in strict accordance with the ethical guidelines of the Declaration of Helsinki and approved by the Ethics Committee of the Children's Hospital of Fudan University (Approval Numbers: FDCH_2022_260 and FDCH_2023_175). All participants were enrolled with informed consent obtained from their parents or legal guardians. Personal information was anonymized, and data were used solely for research purposes, ensuring confidentiality and privacy. The participants had the right to withdraw at any time without penalty. The research team is committed to maintaining data integrity and transparency, and the findings are reported without bias or manipulation.

CRediT authorship contribution statement

Jieyi Chen: Writing – original draft, Project administration, Methodology, Formal analysis, Data curation, Conceptualization. **Siyuan Du:** Writing – original draft, Methodology, Formal analysis, Conceptualization. **Yiting Zhu:** Writing – original draft, Methodology, Formal analysis, Data curation. **Dongyun Li:** Writing – review & editing, Investigation, Data curation. **Chunchun Hu:** Writing – review & editing, Investigation, Data curation. **Lianni Mei:** Writing – review & editing, Investigation, Data curation. **Yunqian Zhu:** Writing – review & editing, Investigation, Data curation. **Huihui Chen:** Writing – review & editing, Investigation, Data curation. **Sijia Wang:** Writing – review & editing, Funding acquisition, Data curation, Conceptualization. **Xiu Xu:** Writing – review & editing, Supervision. **Xinran Dong:** Writing – review & editing, Supervision, Project administration, Funding acquisition, Conceptualization. **Wenhao Zhou:** Writing – review & editing, Supervision, Funding acquisition, Conceptualization. **Qiong Xu:** Writing – original draft, Supervision, Investigation, Funding acquisition, Data curation, Conceptualization.

Data availability

All data relevant to the study are included in the article or uploaded as supplementary information.

Funding

This project was funded by the following grants and contracts: National Key R&D Program of China (2022ZD0116003), The academic leaders development program of Children's Hospital of Fudan University (EKXDPY202306), Foreign expert program of Ministry of Science and Technology (G2022132004L), National Natural Science Foundation of China (82371881 to X. Dong, 32325013 to S. Wang), Three-year action plan for strengthening the construction of the public health system in Shanghai (GWVI-11.2-YQ22); Strategic Priority Research Program of the Chinese Academy of Sciences (XDB38020400); the CAS Project for Young Scientists in Basic Research (YSBR-077); Shanghai Science and Technology Commission Excellent Academic Leaders Program (22XD1424700).

Declaration of competing interest

The authors declare that they have no known competing financial interests or personal relationships that could have appeared to influence the work reported in this paper.

Acknowledgments

We are very grateful to all the participants in this study, as well as those who helped advertise and recruit. We thank all suggestions and comments collected from peers.

Appendix A. Supplementary data

Supplementary data to this article can be found online at https://doi.org/10.1016/j.compbiomed.2025.109912.

References

[1] J.B. Moeschler, M. Shevell, on G. Committee, Comprehensive evaluation of the child with intellectual disability or global developmental delays, Pediatrics 134 (3) (Sep 2014) e903–e918, https://doi.org/10.1542/peds.2014-1839.
[2] R. Hagerman, G. Hoem, P. Hagerman, Fragile X and autism: intertwined at the molecular level leading to targeted treatments, Mol. Autism 1doi (2010), https://doi.org/10.1186/2040-2392-1-12. Artn 12.
[3] J.H. Hersh, R.A. Saul, G. Committee on, Health supervision for children with fragile X syndrome, Pediatrics 127 (5) (May 2011) 994–1006, https://doi.org/10.1542/peds.2010-3500.
[4] S. Kohler, M. Gargano, N. Matentzoglu, et al., The human phenotype ontology in 2021, Nucleic Acids Res. 49 (D1) (Jan 8 2021) D1207–D1217, https://doi.org/10.1093/nar/gkaa1043.
[5] I. Heulens, M. Suttie, A. Postnov, et al., Craniofacial characteristics of fragile X syndrome in mouse and man, Eur. J. Hum. Genet. 21 (8) (Aug 2013) 816–823, https://doi.org/10.1038/ejhg.2012.265.
[6] D.Z. Loesch, M. Lafranchi, D. Scott, Anthropometry in martin-bell syndrome, Am. J. Med. Genet. 30 (1–2) (May-Jun 1988) 149–164, https://doi.org/10.1002/ajmg.1320300113.
[7] D.Z. Loesch, M.L. Sampson, Effect of the fragile-X anomaly on body proportions estimated by pedigree analysis, Clin. Genet. 44 (2) (Aug 1993) 82–88.
[8] Y. Gurovich, Y. Hanani, O. Bar, et al., Identifying facial phenotypes of genetic disorders using deep learning, Nat Med 25 (1) (Jan 2019) 60–64, https://doi.org/10.1038/s41591-018-0279-0.
[9] B. Hallgrimsson, J.D. Aponte, D.C. Katz, et al., Automated syndrome diagnosis by three-dimensional facial imaging, Genet. Med. 22 (10) (Oct 2020) 1682–1693, https://doi.org/10.1038/s41436-020-0845-y.
[10] J.J. Bannister, M. Wilms, J.D. Aponte, et al., Comparing 2D and 3D representations for face-based genetic syndrome diagnosis, Eur. J. Hum. Genet. 31 (9) (Sep 2023) 1010–1016, https://doi.org/10.1038/s41431-023-01308-w.
[11] T.K. Lubala, T. Kayembe-Kitenge, G. Mubungu, et al., Usefulness of automated image analysis for recognition of the fragile X syndrome gestalt in Congolese subjects, Eur. J. Med. Genet. 66 (9) (Sep 2023) 104819, https://doi.org/10.1016/j.ejmg.2023.104819.
[12] V. Biancalana, D. Glaeser, S. McQuaid, P. Steinbach, EMQN best practice guidelines for the molecular genetic testing and reporting of fragile X syndrome and other fragile X-associated disorders, Eur. J. Hum. Genet. 23 (4) (Apr 2015) 417–425, https://doi.org/10.1038/ejhg.2014.185.
[13] E.K. Baker, M. Arpone, S.A. Vera, et al., Intellectual functioning and behavioural features associated with mosaicism in fragile X syndrome, J. Neurodev. Disord. 11 (1) (Dec 26 2019) 41, https://doi.org/10.1186/s11689-019-9288-7.
[14] L. Meng, W.E. Kaufmann, R.E. Frye, et al., The association between mosaicism type and cognitive and behavioral functioning among males with fragile X syndrome, Am. J. Med. Genet. 188 (3) (Mar 2022) 858–866, https://doi.org/10.1002/ajmg.a.62594.
[15] D.Z. Loesch, R.M. Huggins, Q.M. Bui, A.K. Taylor, R.J. Hagerman, Relationship of deficits of FMR1 gene specific protein with physical phenotype of fragile X males and females in pedigrees: a new perspective, Am. J. Med. Genet. 118A (2) (Apr 15 2003) 127–134, https://doi.org/10.1002/ajmg.a.10099.
[16] J.D. White, A. Ortega-Castrillon, H. Matthews, et al., MeshMonk: open-source large-scale intensive 3D phenotyping, Sci. Rep. 9 (1) (Apr 15 2019) 6085, https://doi.org/10.1038/s41598-019-42533-y.
[17] M. Zhang, S. Wu, S. Du, et al., Genetic variants underlying differences in facial morphology in East Asian and European populations, Nat. Genet. 54 (4) (Apr 2022) 403–411, https://doi.org/10.1038/s41588-022-01038-7.
[18] R. Bruggink, F. Baan, S. Brons, et al., A semi-automatic three-dimensional technique using a regionalized facial template enables facial growth assessment in healthy children from 1.5 to 5.0 years of age, PeerJ 10 (2022) e13281, https://doi.org/10.7717/peerj.13281.
[19] H.S. Matthews, R.L. Palmer, G.S. Baynam, et al., Large-scale open-source three-dimensional growth curves for clinical facial assessment and objective description of facial dysmorphism, Sci Rep-Uk 11 (1) (Jun 9 2021) 12175, https://doi.org/10.1038/s41598-021-91465-z.
[20] G.K. Sharma, D.H. Lofgren, M.H. Hohman, H.G. Taliaferro. Recurrent acute rhinosinusitis, StatPearls, 2024. https://www.ncbi.nlm.nih.gov/books/NBK459372/.
[21] W.L. Stone, H. Basit, M. Shah, E. Los. Fragile X syndrome, StatPearls, 2024. https://www.ncbi.nlm.nih.gov/books/NBK459243/.
[22] J.B. Cole, M.F. Manyama, D. Nikitovic, et al., Facial shape manifestations of growth faltering in Tanzanian children, J. Anat. 232 (2) (Feb 2018) 250–262, https://doi.org/10.1111/joa.12748.
[23] M. Arpone, E.K. Baker, L. Bretherton, et al., Intragenic DNA methylation in buccal epithelial cells and intellectual functioning in a paediatric cohort of males with fragile X, Sci. Rep. 8 (1) (Feb 26 2018) 3644, https://doi.org/10.1038/s41598-018-21990-x.
[24] D.E. Godler, H.R. Slater, Q.M. Bui, et al., Fragile X mental retardation 1 (FMR1) intron 1 methylation in blood predicts verbal cognitive impairment in female

carriers of expanded FMR1 alleles: evidence from a pilot study, Clin. Chem. 58 (3) (Mar 2012) 590–598, https://doi.org/10.1373/clinchem.2011.177626.

[25] A.L. Shelton, K.M. Cornish, D. Godler, Q.M. Bui, S. Kolbe, J. Fielding, White matter microstructure, cognition, and molecular markers in fragile X premutation females, Neurology 88 (22) (May 30 2017) 2080–2088, https://doi.org/10.1212/WNL.0000000000003979.

[26] A.L. Shelton, K.M. Cornish, S. Kolbe, et al., Brain structure and intragenic DNA methylation are correlated, and predict executive dysfunction in fragile X premutation females, Transl. Psychiatry 6 (12) (Dec 13 2016) e984, https://doi.org/10.1038/tp.2016.250.